ChemPubSoc Europe

DOI: 10.1002/cphc.201700089

CHEMPHYSCHEM Communications

Gas-Phase Vibrational Spectroscopy of the Aluminum Oxide Anions $(Al_2O_3)_{1-6}AlO_2^-$

Xiaowei Song,[a, b] Matias R. Fagiani,[a, b] Sandy Gewinner,[b] Wieland Schöllkopf,[b] Knut R. Asmis,*[a] Florian A. Bischoff,[c] Fabian Berger,[c] and Joachim Sauer*[c]

We use cryogenic ion trap vibrational spectroscopy in combination with density functional theory to probe how the structural variability of alumina manifests itself in the structures of the gas-phase clusters $(Al_2O_3)_nAlO_2^-$ with $n=1$–6. The infrared photodissociation spectra of the D_2-tagged complexes, measured in the fingerprint spectral range (400–1200 cm^{-1}), are rich in spectral features and start approaching the vibrational spectrum of amorphous alumina particles for $n>4$. Aided by a genetic algorithm, we find a trend towards the formation of irregular structures for larger n, with the exception of $n=4$, which exhibits a C_{3v} ground-state structure. Locating the global minima of the larger systems proves challenging.

The thermodynamically most stable alumina polymorph is α-Al_2O_3 (corundum), but the metastable γ-, η-, θ- and δ-Al_2O_3 phases are also quite common.[1] These various allotropic forms of aluminas have attracted much attention due to their use in various technological applications.[2] They are also a major component of mineral dust aerosols, which influence atmospheric processes like raindrop formation and ice nucleation.[3] The structural variability of aluminas raises the question, how the structure of bulk-like aggregates compares with that of thin films, nanoparticles and smaller gas-phase clusters of the same composition. Here, we address this question on the atomic scale by studying the vibrational spectra of size-selected aluminum oxide clusters with up to 13 Al atoms. Inferences on the atomic structure are made from comparison with spectra predicted by density functional theory (DFT) for minimum-energy structures.

Since charged clusters are required for mass selection we have chosen clusters with the composition $(Al_2O_3)_n(AlO_2)^-$. A formally fully oxidized and electronically closed-shell AlO_2^- moiety was added to the $(Al_2O_3)_n$ formula unit. This way, similar to our previous study on $(Al_2O_3)_nAlO^+$ cations,[4] clusters with unpaired electrons are avoided, whereas the composition converges to that of bulk alumina for large n. Note that the $(Al_2O_3)_n(AlO_2)^-$ sum formula does not imply that the geometric structure is made up of Al_2O_3 building blocks.

The upper part of Figure 1 shows the vibrational spectra of the $(Al_2O_3)_nAlO_2^-$ cluster series with $n=0$ to 6. They were measured by infrared photodissociation (IRPD) spectroscopy of the corresponding D_2-tagged cluster anions. Substantial IR activity above 1000 cm^{-1} is only observed in the IRPD spectra of the two smallest clusters ($n<2$) shown in Figure 1. This range is characteristic for stretching modes of terminal Al–O groups.[5] The clusters with $n\geq 2$ show characteristic absorptions bands in the spectral range from 1000 cm^{-1} down to ≈750 cm^{-1}. The

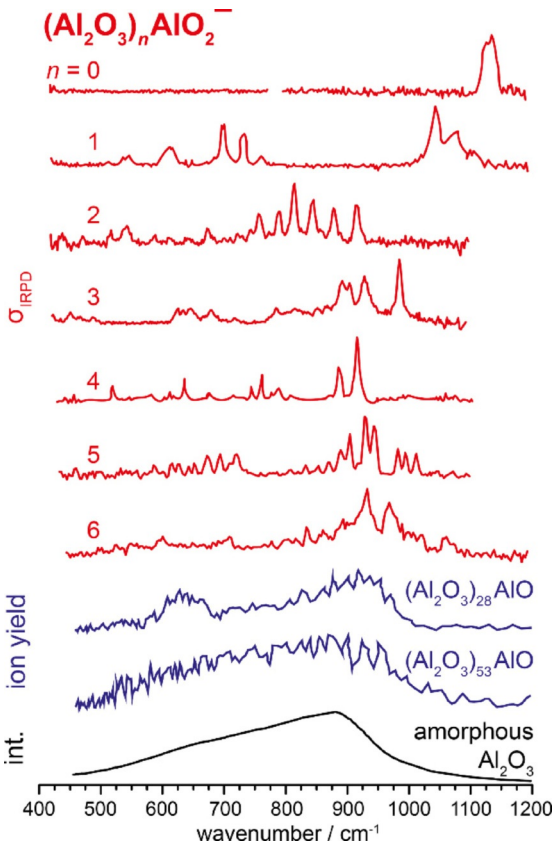

Figure 1. Experimental IRPD spectra (red traces) of D_2-tagged $(Al_2O_3)_{0-6}AlO_2^-$ anions compared with the IR-REMPI spectra (blue traces) of neutral $(Al_2O_3)_{28,53}AlO$ and the IR spectrum (black trace) of amorphous Al_2O_3 derived from the optical constants of bulk aluminum oxide for spherical particles in the Rayleigh limit.[6] The $n=0$ spectrum is reproduced from ref. [5]. See Figure S1 and Table S1 for band positions.

[a] Dr. X. Song, M. R. Fagiani, Prof. Dr. K. R. Asmis
Wilhelm-Ostwald-Institut für Physikalische und Theoretische Chemie
Universität Leipzig, Linnéstrasse 2, 04103, Leipzig (Germany)
E-mail: knut.asmis@uni-leipzig.de

[b] Dr. X. Song, M. R. Fagiani, S. Gewinner, Dr. W. Schöllkopf
Fritz-Haber-Institut der Max-Planck-Gesellschaft
Faradayweg 4–6, 14195, Berlin (Germany)

[c] Dr. F. A. Bischoff, F. Berger, Prof. Dr. J. Sauer
Institut für Chemie, Humboldt-Universität zu Berlin
Unter den Linden 6, 10099, Berlin (Germany)
E-mail: js@chemie.hu-berlin.de

Supporting Information and the ORCID identification number(s) for the author(s) of this article can be found under: http://dx.doi.org/10.1002/cphc.201700089.

spectra of all clusters with $n>0$ show multiple absorption features below 750 cm^{-1} and typically with less intensity compared to the bands at higher energies.

Also shown in Figure 1 are the IR spectra of larger, neutral Al_2O_3 aggregates, including the gas-phase vibrational spectra of $(Al_2O_3)_{28}AlO$ and $(Al_2O_3)_{53}AlO$ measured using infrared resonance-enhanced multiphoton ionization (IR-REMPI) spectroscopy,[6a] as well as a simulated spectrum of amorphous Al_2O_3, derived from the optical constants of bulk aluminum oxide for spherical particles in the Rayleigh limit.[6] The latter two spectra have in common that they show a broad absorption maximum centered around $\approx$900 cm^{-1} with a pronounced tail that extends down to $\approx$500 cm^{-1}, suggesting that aluminum oxide clusters, like $(Al_2O_3)_{53}AlO$, are amorphous-like.[6b]

Inspection of the vibrational spectra of the $(Al_2O_3)_nAlO_2^-$ clusters indeed reveals an evolution of the spectral features with increasing n towards the characteristic IR absorptions of the larger particles. While the IRPD spectra for $n<3$ have little in common with those of the larger aggregates, the strongest IR activity in the $n\geq3$ spectra accumulates around 900 cm^{-1}. Moreover, the IRPD spectra of $n=5$ and $n=6$ show an intensity distribution of their (discrete) absorption features in this spectral region, which is not unlike the intensity profile towards the higher energies of the larger amorphous particles. This similarity may be fortuitous, given the small size and hence low average coordination numbers of the $n=5$ and $n=6$ clusters, but may also be taken as the onset of the evolution of diverse structural motifs similar to those in the larger aggregates. In contrast, the striking simplicity of the $n=4$ spectrum hints at a higher symmetry structure, and its spectrum in fact looks more like the high-resolution electron-energy-loss (HREELS) spectrum of an Al_2O_3/NiAl thin film.[7]

Additional structural information on the $(Al_2O_3)_nAlO_2^-$ clusters can be gained from a comparison with the vibrational spectra of the analogous cationic clusters, $(Al_2O_3)_nAlO^+$, which were studied previously up to $n=4$ using a similar technique, see Figure S2.[4] The IRPD spectra of the anion and the corresponding cation for $n=2$ are strikingly different, suggesting an $Al_5O_8^-$ structure that differs substantially from the conical-like $Al_5O_7^+$ structure identified previously.[4] In contrast, the IRPD spectra for $n=3$ are quite similar, indicating comparable structures. For $n=1$ and $n=4$, the situation is intermediate, suggesting different structures containing similar motifs.

Figure 2 shows the experimental IRPD spectra from Figure 1 together with simulated IR spectra and the corresponding minimum-energy structures obtained by DFT (for computational details see below). The structures are labelled with ***n-a***, where n refers to the number of Al_2O_3 units formally in the cluster and a is an index indicating the energetic ordering for a particular cluster size.

Up to $n=4$, we find satisfactory agreement between the experimental IRPD spectrum and the simulated spectrum of the minimum-energy isomer, whereas the simulated spectra of the higher-energy isomers (see Figures S3–S6) do not agree well, supporting an assignment to the depicted structures. Structure **1-1** is in agreement with the only previous prediction for this cluster series, namely a kite-like structure of C_{2v} symmetry con-

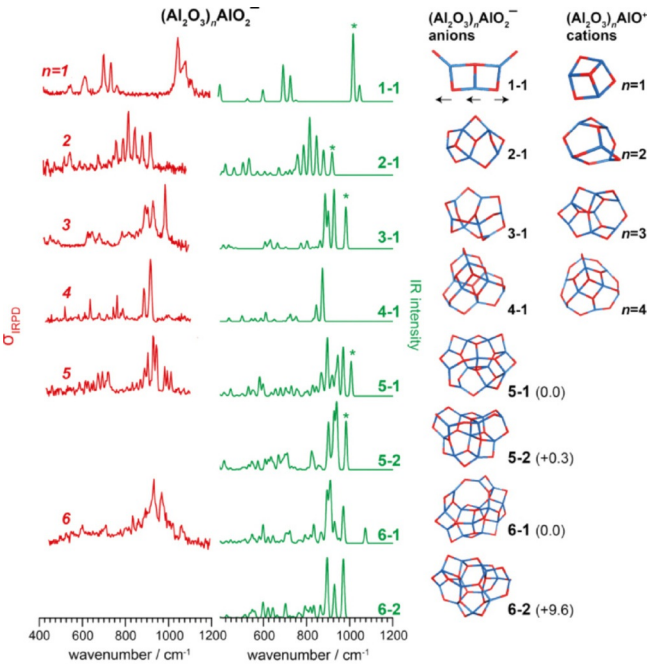

Figure 2. Experimental IRPD spectra (1st column, red traces) of $(Al_2O_3)_nAlO_2^-\cdot D_2$ and computed harmonic IR spectra (2nd column, green traces) of low-energy isomers of $(Al_2O_3)_nAlO_2^-$ for $n=1$–6 (3rd column). Structures (see Section S4 for Cartesian coordinates) and relative energies [kJ mol^{-1}] are shown and compared with their cationic analogs $(Al_2O_3)_nAlO^+$ for $n=1$–4. "*" indicates a band (see Table 3 for band positions) assigned to a normal mode (indicated by the arrows for $n=1$) localized on the T-shaped AlO_3 motif.

taining two characteristic edge-sharing four-membered rings with two terminal Al–O groups.[8] For $n>4$, the simulated spectrum of the minimum-energy structure accounts for most but not all of the observed IRPD bands, suggesting that additional low-energy isomers, such as for example, **5-2** and **6-2,** contribute to the observed IRPD spectra of the larger clusters (see Figures 2, S7 and S8). The variety of structural isomers for $n>4$ makes it increasingly difficult to locate the global minimum structure.

Table 1 shows the average O and Al coordination numbers and the relative coordination number distribution for the O and Al atoms for the low-energy isomers of the $(Al_2O_3)_nAlO_2^-$ clusters. In the following, coordination numbers are stated as superscripts, for example, Al^4 refers to a four-fold coordinated Al-atom. The increasing resemblance of the cluster spectra with those of larger aggregates and that of bulk amorphous alumina with increasing cluster size (see Figure 1) implies that also the cluster structures and hence the average coordination numbers and bond lengths should become more and more similar to those of bulk Al_2O_3.

With the exception of structure **3-1**, the average coordination numbers increase with cluster size, from 1.8 (O) and 3.0 (Al) in **1-1** to 2.5 (O) and 3.85 (Al) in **6-1**, approaching the coordination numbers of amorphous Al_2O_3, 2.1–3.0 (O) and 4.1–4.8 (Al) and of the thin Al_2O_3/NiAl film, 3.0 (O) and 3.9 (Al). In the crystalline bulk phases, the coordination numbers are much higher, between 3.33 and 4 for O, and between 5 and 6 for Al.

Table 1. O/Al ratio, relative coordination number (CN) distribution, and average O and Al coordination numbers for the low-energy isomers of $(Al_2O_3)_nAlO_2^-$ with $n=1$–6 compared to different solid alumina polymorphs. Isomers are labeled with ***n-a***, where *a* refers to the energetic ordering for a particular *n*.

isomer, point group	O/Al ratio	Relative CN distribution								Average CN	
		O^1	O^2	O^3	O^4	Al^3	Al^4	Al^5	Al^6	O^{av}	Al^{av}
1-1, C_{2v}	1.67	0.40	0.40	0.20	0	1	0	0	0	1.80	3.00
2-1, C_1	1.60	0	0.75	0.25	0	0.40	0.60	0	0	2.25	3.60
3-1, C_1	1.57	0	0.91	0.90	0	0.71	0.29	0	0	2.09	3.29
4-1, C_{3v}	1.56	0	0.64	0.36	0	0.33	0.66	0	0	2.36	3.67
5-1, C_1	1.54	0	0.65	0.29	0.06	0.27	0.73	0	0	2.41	3.73
5-2, C_1		0	0.65	0.23	0.12	0.27	0.64	0.09	0	2.47	3.82
6-1, C_2	1.54	0	0.55	0.40	0.05	0.15	0.85	0	0	2.50	3.85
6-2, C_2		0	0.60	0.30	0.10	0.15	0.85	0	0	2.50	3.85
amorphous alumina	1.53[a]									2-3[b]	4-5[b]
thin film[c]	1.3	0	0	1	0	0.40	0.30	0.30	0	3.00	3.90
θ-alumina[d]	1.5	0	0	0.66	0.33	0	0.50	0	0.50	3.33	5.00
γ-alumina[e]	1.5	0	0	0.66	0.33	0	0.40	0	0.60	3.33	5.20
γ-alumina[f]	1.5	0	0	0.66	0.33	0	0.25	0	0.75	3.66	5.50
κ-alumina[g]	1.5	0	0	0.50	0.50	0	0.25	0	0.75	3.50	5.50
α-alumina[h]	1.5	0	0	0	1	0	0	0	1	4	6

[a] Ref. [9]. [b] Ref. [10]. [c] Ref. [11]. [d] Ref. [12]. [e] Spinel, Ref. [13]. [f] Krokidis, Ref. [14]. [g] Ref. [15]. [h] Ref. [16].

Table 2 shows the spread of Al–O bond distances as a function of the respective Al and O coordination numbers for the $(Al_2O_3)_nAlO_2^-$ clusters. The bond distance (strength) tends to increase (decrease) with increasing coordination of the atoms/ions involved in the bond, but no clear trend is seen for Al, because the spread of bond distances is too large. A more detailed table for each isomer is given in Table S5.

Table 2. Al–O bond distances [pm] as a function of the respective Al and O coordination numbers (CN) for $(Al_2O_3)_nAlO_2^-$ clusters (average values, calculated).

CN Al \ CN O	O^2	O^3	O^4
Al^3	168.0–181.8	173.7–185.6	–
Al^4	169.8–182.0	173.4–215.3	183.4–210.0
Al^5	–	173.3–183.5	195.5–207.9

The literature values for Al_2O_3 bulk phases are in line with the present cluster results. In α-Al_2O_3 (corundum) only octahedral sites are filled with coordination Al^6O^4 and bond distances of 185–197 pm.[16] For γ-Al_2O_3, where both tetrahedral and octahedral sites are partially filled,[13,17] the Al^6–O^4 bond distances are in the same range (193 pm), whereas the Al^4–O^4 bond distances are shorter (181 pm), in accord with the larger bond strength due to the lower coordination of Al. Even shorter distances of 171–179 pm have been reported for liquid Al_2O_3 with Al and O coordination numbers of 4-5 and 2-3, respectively.[10a]

Comparison of the cation structures of the $(Al_2O_3)_nAlO^+$ series (see Figure 2) with those of the corresponding anions $(Al_2O_3)_nAlO_2^-$, which differ by an O^{2-} unit, shows more similarities than is expected from the previous comparison of the IRPD spectra (see Figure S2). Indeed, all four cluster pairs ($n=$ 1–4) share characteristic structural motifs. For $n=1$ these are the two edge-sharing four-membered rings containing three three-fold coordinated Al-atoms (Al^3, see Table 1). The additional O atom in the anion leads to two terminal O atoms (O^1) instead of a third edge-sharing four-membered ring in the cation. For $n=2$ three of the five Al^3 centers in the cation are replaced by Al^4 centers with the additional O-atom adding in a triply-coordinated site. For $n=3$ and $n=4$ the extra O atom adds to the center of the conical structure of the cation, replacing the hollow character by a 3D network structure in the anion. Both of these anion structures are unique and quite different from the other structures. Even though the **3-1** structure only has C_1 symmetry, it is rather regular in that it is only composed of six-membered rings with ten O^2, one O^3, five Al^3 and two Al^4 atoms. The absence of smaller rings leads to unusually low average coordination number of $O^{av}=2.1$ and $Al^{av}=3.3$ (see Table 1) in this case. In contrast, **4-1** exhibits a highly symmetric C_{3v} structure, as the simplicity of the corresponding IRPD spectrum already suggested. As a result of the five O^3 and six Al^4 centers, compared to one and two, respectively, for **3-1**, structure **4-1** also exhibits the narrowest bond distance distribution of 170.5–189.9 pm (see Table S2). Finally, the low-energy structures **5-1**, **5-2**, **6-1** and **6-2** are much less regular and indeed their spectra are more amorphous-like. These clusters are the smallest that contain fourfold coordinated O atoms (O^4) and one of them (**5-2**) already contains a fivefold coordinated Al atom (Al^5).

A categorization of the calculated normal modes for each cluster structure is complicated by their delocalized nature. Only the assignment of the higher-energy modes is straightforward. For $n=1$ the highest energy IRPD band at 1074 cm^{-1} can be assigned to the quasi-degenerate symmetric and antisymmetric stretching modes of the two terminal Al-O oscillators, calculated at 1075 cm^{-1} and 1072 cm^{-1}, respectively. The second-highest energy band at 1042 cm^{-1} is thus not a terminal Al–O stretch, but due to an unexpectedly high-lying antisymmetric stretching mode of the O^2–Al^3–O^2 moiety in the $Al(-O)_3$

motif (see Figure 2). Interestingly, similar antisymmetric stretching modes are also present in the spectra of the larger clusters and correspond to the highest energy band (marked with an asterisk in Figure 2) in the spectra of the clusters with $n=2$, 3 and 5. The wavenumber of this mode scales inversely with the average Al^3–O^2 bond length (see Table 3 as well as Table S4 and Figure S9 in the Supporting Information).

Table 3. Experimental and calculated vibrational wavenumbers [cm^{-1}] and distances [pm] of the two Al^3–O^2 bonds of the characteristic T-shaped Al(-O)$_3$ motif in $(Al_2O_3)_nAlO_2^-$. The corresponding bands are marked with an asterisks in Figure 2.

Isomer	Wavenumber		Bond length	
	obsd.	calcd.	Al^3–O^2	average
1-1	1042	1025	168.0, 168.0	168.0
5-1	1011	998	168.3, 169.7	169.0
5-2	994	975	168.1, 170.3	169.2
3-1	985	974	169.3, 169.3	169.3
2-1	916	911	170.7, 171.6	171.2

In conclusion, the assigned structures of the $(Al_2O_3)_nAlO_2^-$ clusters with $n=1$–6 typically contain edge-sharing and corner-sharing four-membered rings as a common structural motif. With the exception of $n=4$, which has C_{3v} symmetry, the larger clusters do not show regular structures. This is reflected in the distribution of coordination numbers for O and Al atoms. The average coordination numbers increase with cluster size, except for $n=3$, and approach those reported for amorphous alumina, as the corresponding IR spectra do.[18]

Experimental Section

Infrared photodissociation experiments are conducted on an ion-trap tandem mass spectrometer described elsewhere.[19] The aluminum oxide anions $(Al_2O_3)_nAlO_2^-$ are either generated using a magnetron sputtering source[20] ($n\leq3$) or a pulsed laser vaporization source[21] for larger clusters ($n=4$–6). In the sputter source, continuous flows of Ar and O_2 buffer gases are injected in front of the Al-sputtering target, while He gas is introduced from the back of the sputtering chamber. Typically, the O_2-to-Ar flow ratio is below 1 to 10 and the total flow results in a pressure range from 10^{-4} to 10^{-3} mbar in the source chamber. Clusters nucleate and grow in a liquid-nitrogen-cooled aggregation zone of adjustable length (10–25 cm) between the target and the source chamber nozzle. To produce larger clusters, the second harmonic output of a 50 Hz Nd:YAG laser is focused onto a moving aluminum rod, and the resulting plasma is entrained in a pulse of 0.5% O_2 in He from a General Valve. Clusters are formed during the subsequent expansion through a clustering channel. The cluster ion beam passes through a 4 mm skimmer, is collimated in a decapole ion guide filled with He as buffer gas and mass-selected using a quadrupole mass-filter. Mass-selected ions are accumulated in a linear radio frequency ring-electrode ion-trap held at 16–30 K and continuously filled with D_2 buffer gas. Trapped ions are internally cooled by collisions with the buffer gas and messenger-tagged with D_2 via three-body collisions: $(Al_2O_3)_nAlO_2^- + 2\,D_2 \rightarrow (Al_2O_3)_nAlO_2^-\cdot D_2 + D_2$.[22] After an ion trap fill time of 199 ms all ions are extracted from the ion trap and focused in the center of the extraction region of a time-of-flight (TOF) mass spectrometer. There they are irradiated by an intense and wavelength-tunable IR laser pulse. When resonant with a vibrational transition parent ions absorb a photon and eventually lose one (or more) messenger molecule(s) via intramolecular vibrational predissociation.

The IR free-electron laser FHI FEL[23] is used as a source for intense and tunable IR radiation. The wavelength of the IR radiation is tuned from 8 to 25 μm with a bandwidth of ca. 0.2% root mean square (rms) of the central wavelength and pulse energies of ≈1 to 12 mJ. IR spectra are recorded by averaging over 90 TOF mass spectra per wavelength step. The intensities are normalized to the total number of parent and fragment ions, to account for fluctuations in the total ion signal. The IRPD cross section σ is determined as described previously.[24]

All calculations were performed with the Turbomole program package.[25] To find the global minimum structures the potential energy surface (PES) was searched by a genetic algorithm[26] (GA) using the BP86 functional[27] together with the split-valence polarized (SVP) basis set (Al:4s3p1d, O:3s2p1d),[28] denoted "def2"-SVP in the Turbomole library. The GA run was repeated five times for 1500 structures, after which convergence was checked. Then the ten lowest-energy structures of the GA were refined using the B3LYP functional[29] with the TZVPP[28] basis set (Al: 5s5p3d1f, O: 5s3p2d1f, named "def2"-TZVPP in the Turbomole library). This basis set was diffuse enough to account for the anionic character of the clusters. No qualitative changes in the geometric and electronic structure were found after refinement. The only exception from this protocol was $(Al_2O_3)_4AlO_2^-$, for which the GA search did not yield structures that were able to explain the IR spectrum. Instead, an educated guess based on the corresponding cationic structure $(Al_2O_3)_4AlO^+$ to which an O^{2-} ion was added, yielded the global energy-minimum structure. All optimized structures were checked for imaginary frequencies and for triplet instabilities. The simulated spectra are derived from computed stick spectra and convoluted with a 10 cm^{-1} fwhm Gaussian line shape function to account for rotational band contours as well as the spectral width of the laser pulse.

Acknowledgements

This research is supported by the Collaborative Research Center 1109 of the German Research Foundation DFG. Xiaowei Song thanks the Alexander-von-Humboldt Foundation for a post-doctoral research fellowship. We thank Prof. Ludger Wöste for providing the magnetron sputter ion source.

Conflict of interest

The authors declare no conflict of interest.

Keywords: aluminium oxide · cryogenic ion trap · density functional theory · gas phase clusters · infrared photodissociation

[1] a) I. Sumio, *Jpn. J. Appl. Phys.* **1984**, *23*, L347; b) I. Levin, D. Brandon, *J. Am. Ceram. Soc.* **1998**, *81*, 1995–2012.
[2] P. Boch, J.-C. Niepce, *Ceramic Materials: Processes, Properties, and Applications*, Wiley, Hoboken, **2010**.

[3] a) P. Warneck, *Chemistry of the Natural Atmosphere*, Elsevier, Amsterdam, **1999**; b) L. Gomes, D. A. Gillette, *Atmos. Environ. Part A* **1993**, *27*, 2539 – 2544.
[4] G. Santambrogio, E. Janssens, S. Li, T. Siebert, G. Meijer, K. R. Asmis, J. Döbler, M. Sierka, J. Sauer, *J. Am. Chem. Soc.* **2008**, *130*, 15143 – 15149.
[5] X. Song, M. R. Fagiani, S. Gewinner, W. Schöllkopf, K. R. Asmis, F. A. Bischoff, F. Berger, J. Sauer, *J. Chem. Phys.* **2016**, *144*, 244305.
[6] a) D. van Heijnsbergen, K. Demyk, M. A. Duncan, G. Meijer, G. von Helden, *Phys. Chem. Chem. Phys.* **2003**, *5*, 2515; b) K. Demyk, D. van Heijnsbergen, G. von Helden, G. Meijer, *Astron. Astrophys.* **2004**, *420*, 547 – 552; c) C. F. Bohren, D. R. Huffman, *Absorption and Scattering of Light by Small Particles*, Wiley-VCH, Weinheim, **2007**.
[7] M. Frank, K. Wolter, N. Magg, M. Heemeier, R. Kühnemuth, M. Bäumer, H.-J. Freund, *Surf. Sci.* **2001**, *492*, 270 – 284.
[8] A. Martínez, F. J. Tenorio, J. V. Ortiz, *J. Phys. Chem. A* **2001**, *105*, 11291 – 11294.
[9] S. K. Lee, S. B. Lee, S. Y. Park, Y. S. Yi, C. W. Ahn, *Phys. Rev. Lett.* **2009**, *103*, 095501.
[10] a) G. Gutiérrez, A. B. Belonoshko, R. Ahuja, B. Johansson, *Phys. Rev. E* **2000**, *61*, 2723 – 2729; b) P. Lamparter, R. Kniep, *Phys. B* **1997**, *234 – 236*, 405 – 406.
[11] G. Kresse, M. Schmid, E. Napetschnig, M. Shishkin, L. Köhler, P. Varga, *Science* **2005**, *308*, 1440 – 1442.
[12] E. Husson, Y. Repelin, *Eur. J. Solid State Inorg. Chem.* **1996**, *33*, 1223 – 1231.
[13] L. Smrčok, V. Langer, J. Křestan, *Acta Crystallogr. Sect. C* **2006**, *62*, i83 – i84.
[14] a) M. Digne, *J. Catal.* **2004**, *226*, 54 – 68; b) X. Krokidis, P. Raybaud, A.-E. Gobichon, B. Rebours, P. Euzen, H. Toulhoat, *J. Phys. Chem. B* **2001**, *105*, 5121 – 5130.
[15] B. Ollivier, R. Retoux, P. Lacorre, D. Massiot, G. Ferey, *J. Mater. Chem.* **1997**, *7*, 1049 – 1056.
[16] L. Lutterotti, P. Scardi, *J. Appl. Crystallogr.* **1990**, *23*, 246 – 252.
[17] R.-S. Zhou, R. L. Snyder, *Acta Crystallogr. Sect. B* **1991**, *47*, 617 – 630.
[18] H. Momida, T. Hamada, Y. Takagi, T. Yamamoto, T. Uda, T. Ohno, *Phys. Rev. B* **2006**, *73*, 054108 – 054108.
[19] D. J. Goebbert, E. Garand, T. Wende, R. Bergmann, G. Meijer, K. R. Asmis, D. M. Neumark, *J. Phys. Chem. A* **2009**, *113*, 7584 – 7592.
[20] I. M. Goldby, B. von Issendorff, L. Kuipers, R. E. Palmer, *Rev. Sci. Instrum.* **1997**, *68*, 3327 – 3334.
[21] T. M. Maier, A. D. Boese, J. Sauer, T. Wende, M. Fagiani, K. R. Asmis, *J. Chem. Phys.* **2014**, *140*, 204315.
[22] K. R. Asmis, T. Wende, M. Brümmer, O. Gause, G. Santambrogio, E. C. Stanca-Kaposta, J. Dobler, A. Niedziela, J. Sauer, *Phys. Chem. Chem. Phys.* **2012**, *14*, 9377 – 9388.
[23] W. Schöllkopf, S. Gewinner, H. Junkes, A. Paarmann, G. von Helden, H. Bluem, A. M. M. Todd, *Proc. SPIE* **2015**, *9512*, 95121L.
[24] a) N. Heine, K. R. Asmis, *Int. Rev. Phys. Chem.* **2015**, *34*, 1 – 34; b) Corrigendum:N. Heine, K. R. Asmis, *Int. Rev. Phys. Chem.* **2016**, *35*, 507.
[25] TURBOMOLE V7.0 2015 a development of University of Karlsruhe and Forschungszentrum Karlsruhe GmbH, 1989 – 2007, TURBOMOLE GmbH, since 2007; available from http://www.turbomole.com.
[26] a) M. Sierka, *Prog. Surf. Sci.* **2010**, *85*, 398 – 434; b) M. Sierka, J. Döbler, J. Sauer, G. Santambrogio, M. Brümmer, L. Wöste, E. Janssens, G. Meijer, K. R. Asmis, *Angew. Chem. Int. Ed.* **2007**, *46*, 3372 – 3375; *Angew. Chem.* **2007**, *119*, 3437 – 3440.
[27] J. P. Perdew, *Phys. Rev. B* **1986**, *33*, 8822 – 8824.
[28] F. Weigend, R. Ahlrichs, *Phys. Chem. Chem. Phys.* **2005**, *7*, 3297 – 3305.
[29] A. D. Becke, *J. Chem. Phys.* **1993**, *98*, 5648.

Manuscript received: January 27, 2017
Accepted Article published: February 24, 2017
Final Article published: March 15, 2017